Journal of Materials Chemistry B

PAPER

View Article Online
View Journal

Cite this: DOI: 10.1039/c4tb01702a

Multiwalled carbon nanotube@reduced graphene oxide nanoribbon heterostructure: synthesis, intrinsic peroxidase-like catalytic activity, and its application in colorimetric biosensing†

Jing Qian,[a] Xingwang Yang,[a] Zhenting Yang,[a] Gangbing Zhu,[b] Hanping Mao[a] and Kun Wang*[a]

Received 15th October 2014
Accepted 6th January 2015

DOI: 10.1039/c4tb01702a

www.rsc.org/MaterialsB

In this study, multiwalled carbon nanotube@reduced graphene oxide nanoribbon (MWCNT@rGONR) core–shell heterostructures have been synthesized by the facile unzipping of MWCNTs and subsequent chemical reduction with hydrazine. MWCNTs with diameter <10 nm were selected as the starting material to maintain narrow ribbons <30 nm wide with a few-layer structure. The most important discovery is that the resulting MWCNT@rGONR heterostructures possess intrinsic peroxidase-like activity, 15.9 times higher than that of MWCNTs and 8.4 times higher than that of their unreduced form. The nature of the peroxidase-like activity of the MWCNT@rGONR heterostructures can be attributed to the acceleration of their electron-transfer process and the consequent facilitation of $^{\bullet}OH$ radical generation. Kinetic analysis demonstrates that the catalytic behavior is in accordance with typical Michaelis–Menten kinetics and the obtained kinetic parameters indicate that the MWCNT@rGONR heterostructures display a higher affinity for both H_2O_2 and 3,3,5,5-tetramethylbenzidine than that of horseradish peroxidase. On this basis, we have employed the MWCNT@rGONR heterostructures as novel biosensing platforms to develop a simple, sensitive, and selective colorimetric biosensor for free cholesterol determination. This work will facilitate the formation of MWCNT@rGONR heterostructures with narrow ribbons and the utilization of their intrinsic peroxidase-like activity in biotechnology and medical diagnostics.

Introduction

Carbon is one of the most abundant elements in our ecosystem, and several novel nanoscale carbon crystalline forms, such as fullerenes, carbon nanotubes (CNTs), and graphene, have been predicted and synthesized over the past few decades.[1,2] Thin and elongated strips of graphene with a high length-to-width ratio and straight edges, termed as graphene nanoribbons (NRs), gradually transform from semiconductors to semimetals as their width increases, and represent a particularly versatile variety of graphene because of the quantum confinement effects.[3,4] The unique characteristics such as high surface areas, high aspect ratios, and interesting electronic properties make graphene NRs promising candidates for applications in synthesizing nanocomposites,[5] hydrogen storage,[6] field-effect transistors,[7] and electrocatalysts.[8] Until now, several attempts have been made to synthesize graphene NRs including chemical,[9,10] sonochemical,[11] and lithographic[12] procedures. Among the graphene NRs produced using the previously described methods, ribbons <100 nm wide are rarely observed in the product.[13] It has to be pointed out that the prevention of aggregation is of particular importance for graphene NRs because most of their unique properties are only associated with individual sheets.[14] The challenge of dispersing graphene NRs has been addressed by the encapsulation of graphene NRs in single-walled CNTs (SWCNTs),[15] or the synthesis of core–shell multiwalled CNT/graphene oxide (GO) NR (MWCNT/GONR) heterostructures.[16–18] In the latter proposal, the individual GONR can possess good stability because the GONR has been planted on the wall of CNTs by the unzipping of MWCNTs. However, except for the enhanced oxygen reduction[8,16] and excellent electrochemical sensing performance,[17,18] there has been little research focused on the peroxidase-like catalytic activity of this kind of heterostructure.

[a]Key Laboratory of Modern Agriculture Equipment and Technology, School of Chemistry and Chemical Engineering, Jiangsu University, Zhenjiang 212013, P. R. China. E-mail: wangkun@ujs.edu.cn; Fax: +86 511 88791708; Tel: +86 511 88791800

[b]School of the Environment and Safety Engineering, Jiangsu University, Zhenjiang 212013, P. R. China

† Electronic supplementary information (ESI) available: Results of the determination of cholesterol in serum samples, typical photographs and absorption spectra of different reaction systems, EIS and CV response corresponding to different electrodes, the typical survey XPS of MWCNT@rGONR heterostructures, CVs of the bare GCE, MWCNT@GONR/GCE, and MWCNT@rGONR/GCE in 50 mM PBS (pH 5.0) at a scan rate of 100 mV s^{-1} in the presence of 50 mM H_2O_2, and selectivity analysis for cholesterol detection. See DOI: 10.1039/c4tb01702a

Currently, colorimetric assays for real-time naked-eye detection have attracted much attention due to their low cost, label-freeness, and simplicity.[19] Since the color changes can be read by the naked eye, colorimetric assays need very little expensive instrumentation or complicated design, and can be performed without trained technicians, making them very attractive for field analysis or point-of-care diagnosis.[19,20] The key challenge for colorimetric assays is the transformation of the detection events into color changes.[21] Generally, natural enzymes have been widely used in the development of colorimetric biosensors due to their high substrate specificity and high catalytic efficiency.[22,23] However, their widespread applications have been restricted by their high-cost of preparation, purification and storage, as well as their low stability due to denaturation.[22,24] As a result, great attention has been focused on the construction and discovery of novel enzyme mimetics for practical applications. Intriguingly, recent studies have shown that some nanomaterials possess intrinsic enzyme mimetic activity similar to that found in natural peroxidases, such as Fe_3O_4 nanoparticles,[25] mesoporous nickel oxide,[26] V_2O_5 nanowires,[27] Co–Al layered double hydroxides,[28] and Au–Cu_xOS yolk–shell nanostructures.[29] Besides metal oxide nanomaterials, SWCNTs,[30] helical CNTs,[31] carboxyl-modified GO,[32] few-layer graphene,[33] and carbon[34] or graphene[35,36] quantum dots of the carbon family are also found to possess intrinsic peroxidase-like catalytic activity. These interesting carbon nanomaterials can catalyze the oxidation of 3,3,5,5-tetramethylbenzidine (TMB) in the presence of H_2O_2 to produce a blue color reaction, which have been employed in the colorimetric sensing of some routine substances such as H_2O_2,[30–34] glucose,[35] and reduced glutathione,[35] thus opening the door for the development of carbon materials in the colorimetric biosensing field.

Cholesterol is an essential lipid found in the human body and plays a vital role in the life of cells, which acts as not only a major structural constituent of plasma membranes, but also a precursor of bile acid, vitamin D, and steroid hormones.[37,38] Actually, the normal concentration of free cholesterol in human serum is in the range of 1.0–2.2 mM.[39] Its abnormal levels might be related to several human diseases including hypertension, maladsorption, arteriosclerosis, brain thrombosis, and myocardial infarction.[40,41] Therefore, developing a method that can quantitatively determine the cholesterol level in blood is very important. Until now, a wide range of methods have been used for the analysis of cholesterol ranging from thin layer chromatography, nuclear magnetic resonance to liquid chromatography-mass spectrometry, and gas chromatography.[40] Although these methods are powerful due to their accuracy and low detection limit, they suffer from the requirement of technical skills and sophisticated instrumentation, as well as the time-consuming procedures involving complicated sample preparation.[42] To this end, the development of inexpensive and operationally simple sensing methods available for rapid parallel analysis of cholesterol would be very interesting and beneficial.[42]

In this work, an improved method is described for the production of MWCNT@reduced graphene oxide NR (MWCNT@rGONR) core–shell heterostructures by the facile unzipped oxidation of MWCNTs, followed by the chemical reduction with hydrazine. MWCNTs with diameter <10 nm were used as the starting material to maintain narrow ribbons <30 nm wide with a few-layer structure. Of particular interest is that the as-obtained MWCNT@rGONR heterostructures exhibited high peroxidase-like activity, which was found to follow Michaelis–Menten kinetics, and also showed a higher affinity for both H_2O_2 and TMB than that of horseradish peroxidase (HRP). On this basis, we have, for the first time, employed the MWCNT@rGONR heterostructures as novel biosensing platforms to develop a simple, sensitive, and selective colorimetric method for free cholesterol determination.

Experimental section

Materials

MWCNTs (diameter <10 nm) were purchased from Shenzhen Nanotech Port Co., Ltd. $KMnO_4$, H_2SO_4 (98.4%), H_3PO_4, H_2O_2, hydrazine solution, ammonia solution, TMB, Triton X-100, cholesterol, glucose, ascorbic acid (AA), lactic acid, and L-cysteine were purchased from Sinopharm Chemical Reagent Co. Ltd. Cholesterol oxidase (COx) and *tert*-butyl alcohol were obtained from Sigma-Aldrich. All the reagents were used as purchased without further purification. Double-distilled water was used throughout the study.

Apparatus

The morphologies of the samples were analyzed with a transmission electron microscope (TEM, Hitachi S-2400N, Japan). Fourier transform infrared (FT-IR) spectra were recorded using a Nicolet Nexus 470 FT-IR spectrophotometer (Thermo Nicolet, USA). Raman spectra were recorded on a RM 2000 microscopic confocal Raman spectrometer (Renishaw inVia Plus, England). The UV-vis spectra and the time-dependent absorbance changes were recorded on an Analytik Jena SPECORD S600 UV-vis spectrometer (Germany). X-ray photoelectron spectroscopy (XPS) was performed on an ESCALAB 250 multitechnique surface analysis system (Thermo Electron Co., USA). The inductively coupled plasma (ICP) spectroscopic detection of the Mn element in the MWCNT@rGONR sample was performed on a Vista-MPX inductively coupled plasma spectrometer (VARIAN Co. USA). The electrochemical impedance spectra (EIS) were recorded over the frequency range of 10 kHz to 0.01 Hz in 5 mM $[Fe(CN)_6]^{3-/4-}$ containing 0.1 M KCl at room temperature. The cyclic voltammograms (CVs) were recorded in deoxygenated PBS (50 mM, pH 5.0) at room temperature. All the electrochemical experiments were performed with a computer-controlled electrochemical analyzer (CHI 660B, CHI Instrument, China) in a conventional three-electrode system composed of a glassy carbon electrode (GCE, 3 mm in diameter) as the working electrode, platinum wire as the counter electrode, and a saturated calomel electrode as the reference electrode.

Preparation of MWCNT@rGONR core–shell heterostructures

For producing MWCNT@GONR heterostructures,[13,43] 120 mg of MWCNTs was dispersed in 40 mL of H_2SO_4/H_3PO_4 (9 : 1, v/v)

under stirring for 1 h and the mixture was then heated at 65 °C followed by stirring for another 2 h after the addition of 600 mg of $KMnO_4$. Then the mixture was allowed to cool to room temperature and poured into 400 mL of ice water containing 5 mL of 30% H_2O_2 to prevent the precipitation of insoluble MnO_2. The solutions were filtered through a polytetrafluoroethylene membrane (0.2 μm pore size), and the resulting solids were washed with acidic water (20 vol% concentrated HCl) and water several times, followed by drying at 50 °C in vacuum.

For producing MWCNT@rGONR heterostructures, 10 mL of the above solid product suspension (0.5 mg mL^{-1}) was mixed with 10 μL of hydrazine solution and 70 μL of ammonia solution followed by stirring for 10 min. After the mixture was stirred at 60 °C for an additional 3.5 h, the reaction solution was cooled down to room temperature and dialyzed to remove the excess hydrazine. Finally, the above suspension was dried at 50 °C in vacuum to obtain the MWCNT@rGONR core–shell heterostructures.

Peroxidase-like catalytic activity study

5 μg of MWCNT@rGONR heterostructures, 0.1 mmol of H_2O_2, and 0.8 μmol of TMB were mixed with PBS (50 mM, pH 5.0) to a final volume of 1 mL. Then the absorption spectra and photographs were recorded after the mixture was incubated for 15 min at 30 °C in a water bath.

Kinetic analysis

Kinetic measurements were carried out in time-drive mode by monitoring the absorbance change at 652 nm. Unless otherwise stated, experiments were carried out using 5 μg mL^{-1} MWCNT@rGONR in a reaction volume of 1 mL PBS (50 mM, pH 5.0), with 0.8 mM of TMB and 0.1 M of H_2O_2 as substrates at 30 °C. The Michaelis–Menten constant was calculated using Lineweaver–Burk plots of the double reciprocal of the Michaelis–Menten equation, $1/v = (K_m/V_{max})(1/[S]) + 1/V_{max}$, where v is the initial velocity, [S] is the concentration of the substrate, K_m is the Michaelis–Menten constant, and V_{max} is the maximal reaction velocity.

$^{\cdot}$OH radical measurements

5 μg mL^{-1} of MWCNT@rGONR, 0.1 mmol of H_2O_2, and 1 mmol of *tert*-butyl alcohol were mixed with PBS (50 mM, pH 5.0) to a final volume of 960 μL. After the mixture being incubated at room temperature for 30 min, 0.8 μmol TMB dissolved in 40 μL was added. The UV-vis spectrum was recorded after the above mixture was incubated for another 15 min at 30 °C in a water bath. For comparison, the absorption spectrum of the MWCNT@rGONR + H_2O_2 + TMB solution was also measured under the same conditions by replacing the *tert*-butyl alcohol.

Fabrication of the MWCNT@rGONR modified electrodes

5 μL of 0.5 mg mL^{-1} MWCNT@GONR and MWCNT@rGONR suspension was cast onto the pretreated GCE surface and dried in air at room temperature, to obtain the MWCNT@GONR/GCE and MWCNT@rGONR/GCE, respectively.

Colorimetric biosensing of free cholesterol

The colorimetric detection of free cholesterol was performed by a very simple process. Specifically, different concentrations of cholesterol containing 0.2% (v/v) Triton X-100 were first mixed with 0.5 unit of Cox, 5 μg of MWCNT@rGONR, and 0.1 mmol of H_2O_2 in 1 mL PBS (50 mM, pH 5.0) using 0.8 mM TMB as the colorimetric substrate. Then the absorbance at 652 nm and photographs of the reaction solution were recorded after incubation for 30 min at 35 °C in a water bath.

Results and discussion

Characterization of the MWCNT@rGONR core–shell heterostructures

Raman spectra were employed for evaluating the structure of the heterostructures before and after the chemical reduction with hydrazine (Fig. 1A). The as-received MWCNTs (curve a) exhibited typical D and G bands at 1340 and 1580 cm^{-1} with the D/G intensity (I_D/I_G) ratio of 0.45. Similar to what has been reported for GONR,[13] the G band of MWCNT@GONR (curve b) broadened and shifted to 1605 cm^{-1} with the appearance of the D band at 1348 cm^{-1}. In addition, the I_D/I_G ratio (0.99) of MWCNT@GONRs was much greater than that of MWCNTs, demonstrating a decrease in the size of the sp^2-hybridized carbon domain during the unzipping process. In agreement with previous reports for chemically reduced GONRs,[44] the I_D/I_G ratio (1.51) remarkably increased after conversion to MWCNT@rGONR heterostructures (curve c).[45] It is hypothesized that the reduction increases the number of small domains of aromaticity responsible for the D peak, but not necessarily their overall size responsible for the G peak.[45]

The oxidation–reduction process of MWCNT@GONR was also evidenced by the FT-IR spectra (Fig. 1B). The MWCNTs (curve a) exhibited typical C=C conjugation and C–C bands at 1635 and 1050 cm^{-1}, respectively.[46] The FT-IR spectra of the MWCNT@GONR (curve b) exhibited several characteristic peaks of C=O stretching of COOH groups (1715 cm^{-1}), O–H bending vibration, epoxide groups and skeletal ring vibrations (around 1570 cm^{-1}), and tertiary C–OH groups (1400 cm^{-1}).[47] The weak C=O stretching characteristic peak (1715 cm^{-1}) suggested that MWCNT@rGONR (curve c) had been partially reduced by hydrazine,[47] which was consistent with the Raman results. The absorption band at 1625 cm^{-1} might be assigned to

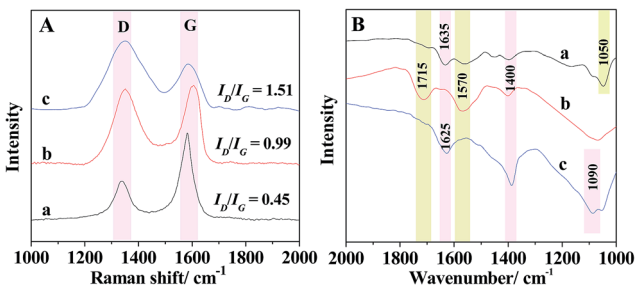

Fig. 1 Raman spectra (A) and FT-IR spectra (B) of MWCNTs (a), WCNT@GONR (b), and MWCNT@rGONR (c).

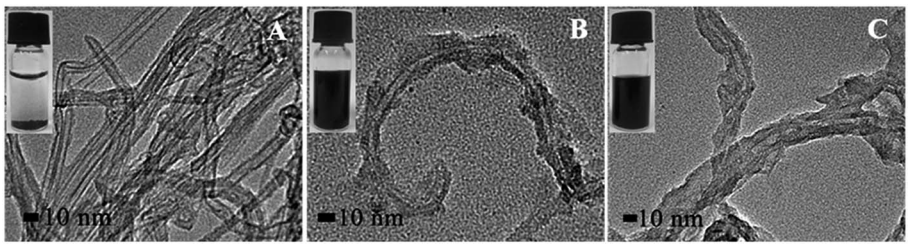

Fig. 2 TEM images of MWCNTs (A), MWCNT@GONR (B), and MWCNT@rGONR (C).

the stretching vibration of the C=C of MWCNT@rGONR and another band at 1090 cm^{-1} could be assigned to the stretching vibration of the C–O.[48] These C–O bonds coming from some defects including oxygen atoms in the MWCNT@rGONR could not be removed completely from the heterostructures by chemical reduction methods.[48]

The morphologies of the as-received MWCNTs (A) and the as-produced MWCNT@GONR (B) and MWCNT@rGONR (C) nanostructure were all examined using TEM images (Fig. 2). The pristine MWCNTs (Fig. 2A) presented a dense and tube-like structure entwined with each other, and the diameter of a single MWCNT was less than 10 nm, which could not form a stable suspension in water even after ultrasonic treatment for several hours, thus leading to serious precipitation and strong aggregation (inset of Fig. 2A). After the pristine MWCNTs were oxidized and unzipped by treatment with H_2SO_4/H_3PO_4 with dissolved $KMnO_4$ (Fig. 2B), thinner ribbon-like graphene wings were formed on both sides of the nanotubes with less MWCNT inner tube remaining in successive iterations, whereas the central cores of the nanotubes remained slightly dark and tubular structure. Unlike the poor dispersity of MWCNTs, the MWCNT@GONR dispersion was stable for more than four weeks with no obvious aggregation (inset of Fig. 2B). Since the unzipping process was oxidative, the resulting MWCNT@GONR possessed enriched oxygen-containing functionalities at the edge and surface of the graphene-like framework, evidenced by the above FT-IR spectra, which could be responsible for its extraordinary dispersity in water.[17] Similar to the reduction of GO, the resulting MWCNT@GONR could be reduced by the chemical method resulting in significantly lower oxygen content and restoration of much of the π–π conjugation, noted by an increase in electrical conductivity.[44] After reduction with hydrazine, the core–shell heterostructure remained and the morphology of the MWCNT@rGONR (Fig. 2C) showed no difference from that of the MWCNT@GONR. As with the rGO nanosheet, the individual rGONRs tended to form irreversible agglomerates through π-stacking and van der Waals interactions. However, the black dispersion of MWCNT@rGONR was very homogeneous and stable at room temperature upon storage for four weeks (inset of Fig. 2C). It is hypothesized that the unique structure of MWCNT@rGONR in which the rGONR planted on the wall of the tube was advantageous for inhibiting aggregation. A considerable number of residual surface oxygen groups were also responsible for its good dispersity and stability.

Peroxidase-like activity of the MWCNT@rGONR heterostructures

To demonstrate the peroxidase-like activity of the MWCNT@rGONR heterostructures, catalytic oxidation of the peroxidase substrate, TMB, in the presence or absence of H_2O_2 was investigated (Fig. 3). As can be observed, the MWCNT@rGONRs could catalyze the oxidation of TMB by H_2O_2 to produce the reaction solution possessing a typical blue color (photograph a in Fig. 3A). The maximum absorbance of the reaction mixture was 652 nm (curve a in Fig. 3A), which arose from the oxidation product of TMB (oxTMB).[49] In contrast, the MWCNT@rGONR + TMB system showed negligible color variation (photograph b in Fig. 3A) with an insignificant absorbance in the measured range (curve b in Fig. 3A), while the TMB + H_2O_2 system without MWCNT@rGONR was colorless (photograph c in Fig. 3A) and presented a negligible absorption in the range of 500 to 800 nm (curve c in Fig. 3A). These results supported that the MWCNT@rGONR heterostructures possessed intrinsic peroxidase-like activity.

It has been proved that MnO_2 itself also has the peroxidase-like activity,[50] to confirm whether there was MnO_2 in the product, significant information on the chemical composition of the resulting MWCNT@rGONR heterostructures was obtained using XPS measurements. The typical survey XPS of MWCNT@rGONR heterostructures (Fig. S1†) clearly indicated that the sample was composed of C and O elements, and no peaks of other elements were observed, suggesting that the as-prepared MWCNT@rGONR heterostructures were of high purity. Besides, the MWCNT@rGONR heterostructures were further dissolved using aqua regia and the content of Mn^{2+} was then determined by ICP spectrometry. The experimental results revealed that there was no

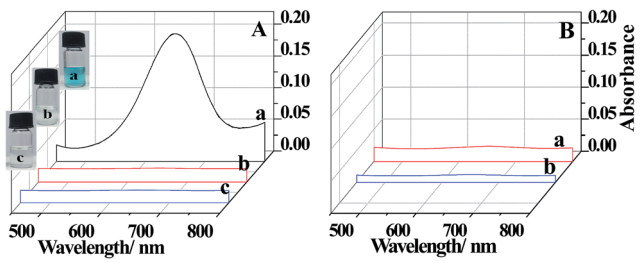

Fig. 3 (A) Typical photographs and absorption spectra of MWCNT@rGONR + TMB + H_2O_2 (a), MWCNT@rGONR + TMB (b), and TMB + H_2O_2 (c). (B) The absorption spectra of MWCNT@GONR + TMB + H_2O_2 (a) and MWCNT + TMB + H_2O_2 (b).

Mn^{2+} in the sample. Both the XPS and ICP results confirmed that no MnO_2 or Mn^{2+} remained in the MWCNT@rGONR product. We can draw the conclusion that the peroxidase-like catalytic activity of the resulting MWCNT@rGONR heterostructures originated from themselves indeed.

More importantly, we compared the catalytic efficiencies of MWCNT@rGONR, MWCNT@GONR (curve a in Fig. 3B), and MWCNTs (curve b in Fig. 3B). The results clearly indicated that MWCNT@rGONR had much better catalytic performance under the same experimental conditions; its catalytic activity was 8.4 times higher than that of MWCNT@GONR and 15.9 times higher than that of MWCNTs. The high catalytic activity of the as-obtained MWCNT@rGONR might be attributed to its high conductivity, because a considerable number of surface oxygen groups have been removed under the action of the reducing agent, resulting in a lower number of defects on the surface.[33]

In order to further understand the high catalytic activity of the MWCNT@rGONR, the electrochemical properties of the as-obtained MWCNT@GONR and MWCNT@rGONR were investigated by EIS exploiting the solution-based redox probe $[Fe(CN)_6]^{3-/4-}$ (Fig. S2A†). In the EIS, the semicircle portion observed at high frequencies corresponded to the electron transfer resistance (R_{et}) and its value could be directly measured as the semicircle diameter. The R_{et} of the MWCNT@GONR/GCE (curve b in Fig. S2A†) dramatically increased as compared to that of the bare GCE (curve a in Fig. S2A†), suggesting that the MWCNT@GONR served as an insulating layer which made the interfacial electron transfer difficult due to its disrupted sp^2 bonding network.[51] Compared with that of the MWCNT@GONR/GCE, an obvious decrease of R_{et} was observed from the MWCNT@rGONR/GCE (curve c in Fig. S2A†), indicating that the as-obtained MWCNT@rGONR could accelerate the electron transfer between $[Fe(CN)_6]^{3-/4-}$ and the electrode.[51] The main reason was attributed to the significantly improved electrical conductivity of MWCNT@rGONR after the reduction process, presumably owing to the restoration of a graphitic network of sp^2 bonds.[51] From the corresponding CV characterization (Fig. S2B†), the peak currents increased and the peak-to-peak separation decreased from curves a to c, which was in good agreement with that of the EIS studies.

Dependence of the peroxidase-like activity

Similar to the natural peroxidase, the catalytic activity of MWCNT@rGONR was dependent on the pH and temperature. PBS was selected for the catalytic reaction, and a series of PBS solutions with varied pH values were investigated (Fig. 4A). Higher catalytic activity was obtained in weakly acidic solutions (pH 4.0–5.0) than that in neutral and strong acidic solutions and the optimum solution pH was 5.0. In the temperature range between 25 and 40 °C, MWCNT@rGONR showed a stable catalytic activity, and the catalytic activity decreased when the temperature continued rising, which could be attributed to the decomposition of H_2O_2 at higher temperature (Fig. 4B). The catalytic activity of MWCNT@rGONR was also related to its amount and the concentration of TMB and H_2O_2. The study on the effect of the catalyst amount (Fig. 4C) showed that the

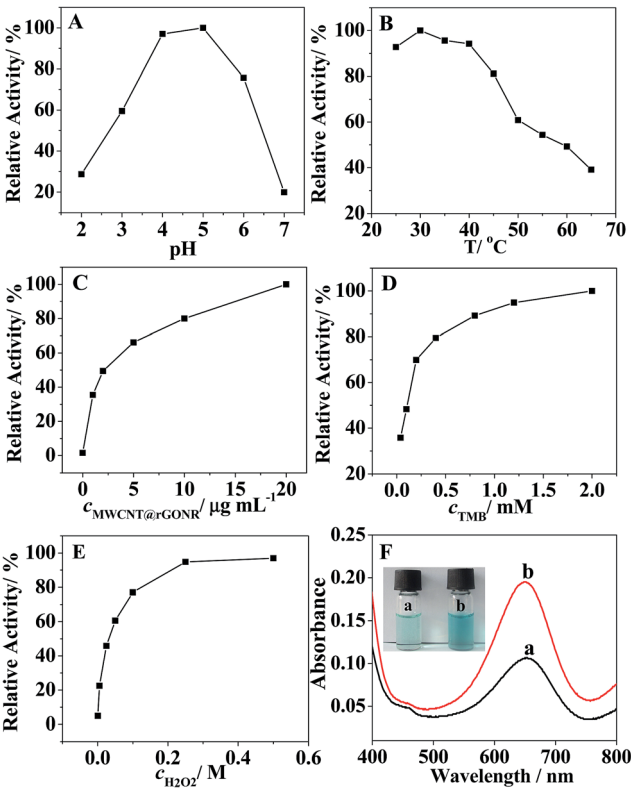

Fig. 4 Dependence of the peroxidase-like activity on pH (A), temperature (B), TMB concentration (C), MWCNT@rGONR amount (D), and H_2O_2 concentration (E). (F) Comparison of the catalytic activity of the MWCNT@rGONR with (a) and without (b) prior incubation with *tert*-butyl alcohol.

catalytic activity increased quickly from 1 to 5 μg mL^{-1} and slowed down beyond 5 μg mL^{-1}. Taking TMB substrate concentration into account (Fig. 4D), the results showed that the relative activity leveled off at the concentrations greater than 0.8 mM. Similar to that of porphyrin-carbon nanoparticle composites,[52] no inhibition of catalytic activity was observed at high H_2O_2 concentration for MWCNT@rGONR-catalyzed reaction, indicating that the catalytic activity of the MWCNT@rGONR was more stable at high H_2O_2 concentration than that of HRP (Fig. 4E).[22] Taking all of the experimental results into consideration, the optimized catalytic conditions were approximately pH 5.0, 30 °C, 5 μg mL^{-1} of MWCNT@rGONR, 0.8 mM of TMB, and 0.1 M of H_2O_2.

Mechanism of the peroxidase-like activity of MWCNT@rGONR

Unlike the typical Fe_3O_4, Co_3O_4, and CeO_2 nanoenzymes, the mechanism of peroxidase-like activity of carbon materials has not been well understood. Considering that the nature of the peroxidase-like activity of most enzyme mimetics may originate from their catalytic ability to decompose H_2O_2 into $^{\bullet}OH$ radicals,[20,53,54] the $^{\bullet}OH$ formation was assessed by introducing *tert*-butyl alcohol as a typical $^{\bullet}OH$ radical capture reagent into the MWCNT@rGONR + H_2O_2 + TMB reaction system (Fig. 4F). The experimental results showed the absorbance intensity of the

solution with the prior introduction of *tert*-butyl alcohol was much lower than that without the introduction of *tert*-butyl alcohol, indicating that MWCNT@rGONR could decompose H_2O_2 to generate the $^{\bullet}OH$ radicals.[54] Like the peroxidase mimics with iron centers, we think that the electron transfer occurred between pairs of different oxidation states of MWCNT@rGONRs may drive their catalytic activity, consistent with that reported for graphene quantum dots.[36] A possible catalytic mechanism of MWCNT@rGONRs could be deduced from Scheme S1†.[55] First, H_2O_2 molecules were adsorbed onto the surface of MWCNT@rGONRs and then catalyzed by the MWCNT@rGONRs which acted as a peroxidase to produce $^{\bullet}OH$ radicals, and the produced $^{\bullet}OH$ radicals were stabilized by MWCNT@rGONRs *via* partial electron exchange interactions. Secondly, TMB was oxidized by $^{\bullet}OH$ radicals to form a blue-colored product. The blue signal came from the charge transfer complex (chromogen), consisting of a cation free radical $TMB^{+\bullet}$ and TMB.

Moreover, we also measured the electrocatalytic behavior of the MWCNT@GONR and MWCNT@rGONR modified GCE towards the electrochemical reduction of H_2O_2 using amperometric responses (Fig. S3†). Obviously, the MWCNT@rGONR modified electrode has the largest current intensity, which demonstrated that the as-obtained MWCNT@rGONR displayed excellent electrocatalytic activity towards H_2O_2 reduction. That is, MWCNT@rGONR had the ability to promote electron transfer between the electron donor (the underlying electrode) and the electron acceptor (H_2O_2).[33] The difference of reduction current between the MWCNT@GONR/GCE and the MWCNT@rGONR/GCE might be due to the great electrical conductivity of MWCNT@rGONR which further induced the increase of electron transfer rate.[53] The structural investigation of the MWCNT@rGONR demonstrated that a considerable amount of carboxylic/carbonyl moieties remained on its surface (Fig. 1B). A density functional theory study also indicated that the functionalization of graphene surfaces with carboxylic groups is significant for H_2O_2 reduction.[56] It is speculated that a similar effect may be observed for the peripherally functionalized carboxylic/carbonyl moieties in the MWCNT@rGONR.[34] To conclude, an increase in the electron density and mobility of MWCNT@rGONR due to electron transfer from lone-pair electrons in TMB amino groups to MWCNT@rGONR could also responsible for its catalytic activity. This would result in the acceleration of electron transfer from the MWCNT@rGONR to H_2O_2, accompanied by an increase of the reaction rate of TMB oxidation by $^{\bullet}OH$ radicals.[34] Based on the above discussions, we can conclude that the peroxidase-like activity of the MWCNT@rGONR heterostructures was attributed to the acceleration of their electron-transfer process and the consequent facilitation of $^{\bullet}OH$ radical generation.[53]

Kinetic analysis of the MWCNT@rGONR heterostructures

In order to acquire the apparent steady-state kinetic parameters for MWCNT@rGONR, a series of experiments were performed by varying the concentration of one substrate and fixing the concentration of the other substrate. In a certain concentration range of substrate, typical Michaelis–Menten curves were received for TMB (Fig. 5A) and H_2O_2 (Fig. 5B), respectively. A series of initial reaction rates were calculated and applied to the double reciprocal of the Michaelis–Menten equation. The K_m and V_{max} were calculated using Lineweaver–Burk plots and are listed in Table 1. As we all know, K_m is identified as an indicator of enzyme affinity for a substrate. A smaller value of K_m stands for a stronger affinity and *vice versa*.[22] By comparing the apparent kinetic parameters, it was found that the K_m value of MWCNT@rGONR with TMB as the substrate was 3.5 times lower than that of HRP, indicating that the MWCNT@rGONR heterostructures had higher affinity for TMB than HRP. This might be due to the advantages of MWCNT@rGONR heterostructures such as their larger surface area, higher conductivity, and stronger adsorption ability for TMB. The K_m value of the MWCNT@rGONR with H_2O_2 as the substrate was slightly higher than that of HRP, suggesting that the MWCNT@rGONR had higher affinity for H_2O_2 than HRP. This would result in high activities and wide-ranging applications.

Colorimetric biosensing applications

In order to evaluate the applicability of the proposed method based on the MWCNT@rGONR heterostructure as a peroxidase

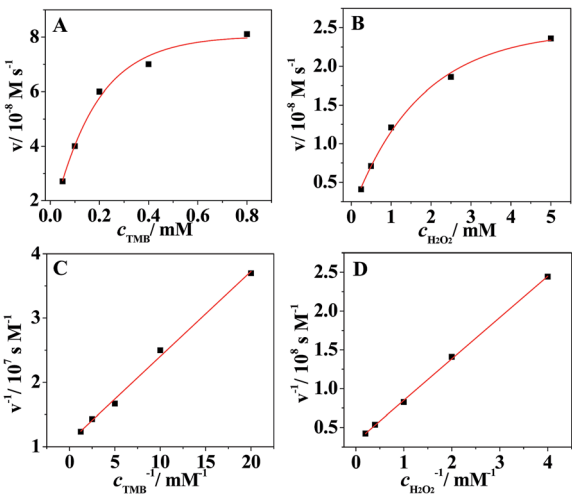

Fig. 5 Steady-state kinetic assay of MWCNT@rGONR. The velocity of the reaction was measured using 10 μg mL^{-1} of MWCNT@rGONR in 50 mM PBS (pH 5.0) at 30 °C. (A) The concentration of TMB was 0.8 mM and the concentration of H_2O_2 was varied. (B) The H_2O_2 concentration was 100 mM and the TMB concentration was varied. Double reciprocal plots of the activity of MWCNT@rGONR at a fixed concentration of H_2O_2 (C) or TMB (D) *versus* varying concentrations of the other.

Table 1 The kinetic parameters of MWCNT@rGONR

	K_m/mM		$V_{max}/10^{-8}$ M s^{-1}	
Catalyst	H_2O_2	TMB	H_2O_2	TMB
MWCNT@rGONR	1.68	0.12	3.15	9.28
HRP[25]	3.7	0.43	8.71	10.0

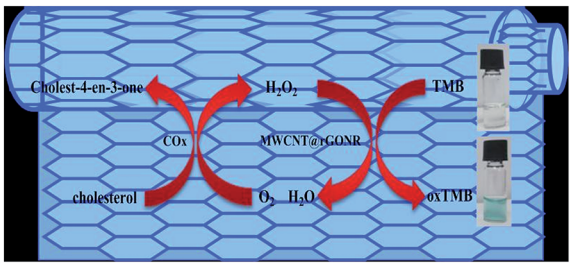

Scheme 1 Schematic illustration of the colorimetric biosensor for cholesterol based on the MWCNT@rGONR heterostructures.

mimetic, we designed a simple colorimetric biosensor for free cholesterol, since H_2O_2 could be generated in the presence of COx in the cholesterol containing solution, and the absorbance of the chromogen in the presence of MWCNT@rGONR was dependent on the H_2O_2 concentration. As illustrated in Scheme 1, cholesterol was converted to cholest-4-*en*-3-one and H_2O_2 by COx and the TMB was further oxidized by the as-produced H_2O_2 in the presence of MWCNT@rGONR producing the blue-colored chromogen, and the absorbance intensity of the reaction solution was directly proportional to the H_2O_2 concentration. Therefore, the color change and the absorbance from oxTMB were dependent on the concentration of cholesterol.

The results showed that the color variation of the reaction solution for increasing amounts of cholesterol displayed continuous color changes from light to deep, which could be clearly observed by the naked eye (Fig. 6A). Moreover, the absorbance intensity at 652 nm increased gradually with the increasing concentrations of cholesterol (Fig. 6B). By analyzing the absorbance intensity (I) *versus* the concentrations of cholesterol (Fig. 6C), we obtained a linear curve that fitted to a regression equation of $I = 1.2512c - 0.0027$ ($R^2 = 0.9850$) over a range of 20 μM to 1 mM with a detection limit of 10 μM at $S/N = 3$. The reproducibility of the biosensor was evaluated by measuring the absorbance for 500 μM cholesterol in the sensing system. For a series of five solutions prepared in the same way, a relative standard deviation of 5.7% was obtained, indicating that this method had good reproducibility.

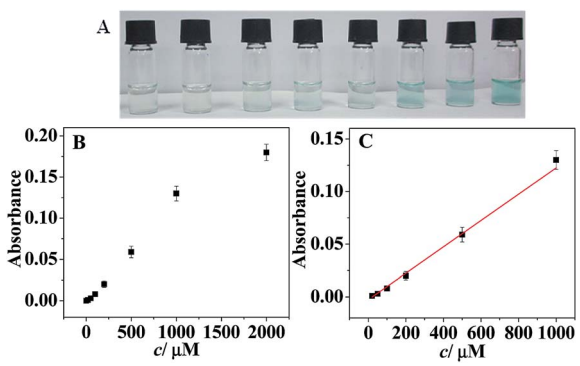

Fig. 6 Photographs (A) and absorbance (B) of the reaction solution for different cholesterol concentrations, from left to right: 0, 20, 50, 100, 200, 500, 1000, and 2000 μM. (C) The linear calibration plot for free cholesterol.

The specificity of the proposed method was tested using normal concentrations of interferents such as L-cysteine (5 mM), lactic acid (5 mM), AA (5 mM), and glucose (5 mM) (Fig. S4†). The color difference for these interferents could also be distinguished by the naked eye. This demonstrated biosensing system was selective for cholesterol detection. However, it is reported that the addition of AA to H_2O_2 can result in the reduction of $TMB^{+\bullet}$ to TMB and the color changes from blue to colorless.[57] The results of our control experiments also showed that the absorbance of 1 mM cholesterol + a high concentration of AA (>10 mM) was much lower than that of the cholesterol only, while its influence could be ignored at a lower concentration (<1 mM). As the normal physiological level of AA is 0.1 mM,[58] the proposed sensing method can be applied to determine the cholesterol level in human serum samples.

To test the cholesterol response on application of this biosensing system, the standard addition method was followed for different serum samples, and the free cholesterol concentration in these real samples was determined from the calibration curve. The recovery results indicated that the as-proposed colorimetric biosensing system had promising potential for practical application in serum samples (Table S1†).

Conclusions

In summary, MWCNT@rGONR maintaining narrow ribbons <30 nm wide was successfully prepared by the unzipped oxidation of MWCNTs and the subsequent chemical reduction with hydrazine. The most important discovery is that the resulting MWCNT@rGONR heterostructure has a higher peroxidase-like activity than that of MWCNTs and its unreduced form. The results of the catalytic mechanism study showed that the peroxidase-like activity of the MWCNT@rGONR heterostructures is attributed to the acceleration of their electron-transfer process and the consequent facilitation of $^{\bullet}OH$ radical generation. Kinetic analysis indicates that the catalysis is in accordance with the Michaelis–Menten kinetics and the kinetic parameters indicate that the MWCNT@rGONR heterostructures have a higher affinity for both H_2O_2 and TMB than that of HRP. On this basis, we have, for the first time, employed the MWCNT@rGONR heterostructures as biosensing platforms to develop a simple, sensitive, and selective colorimetric method for free cholesterol determination. As a novel peroxidase mimetic, the resulting MWCNT@rGONR core–shell heterostructure exhibits a great degree of potential for use as an excellent colorimetric biosensing platform in a variety of fields.

Acknowledgements

The present work was supported by the National Natural Science Foundation of China (no. 21175061, 21375050, and 21405063), the Natural Science Foundation of Jiangsu province (no. BK20130481), Qing Lan Project, a Project Funded by the Priority Academic Program Development of Jiangsu Higher Education Institutions (no. PAPD-2014-37), the Scientific Research Foundation of Jiangsu University (no. 12JDG087), and

the Key Laboratory of Modern Agriculture Equipment and Technology (no. NZ201109 and NZ201307).

Notes and references

1 C. Chung, Y. K. Kim, D. Shin, S. Ryoo, B. H. Hong and D. H. Min, *Acc. Chem. Res.*, 2013, **46**, 2211–2224.
2 C. Z. Zhu, J. F. Zhai and S. J. Dong, *Nanoscale*, 2014, **6**, 10077–10083.
3 S. D. Wang and J. L. Wang, *J. Phys. Chem. C*, 2012, **116**, 10193–10197.
4 H. Ago, Y. Ito, M. Tsuji and K. Ikeda, *Nanoscale*, 2012, **4**, 5178–5182.
5 M. A. Rafiee, W. Lu, A. V. Thomas, A. Zandiatashbar, J. Rafiee, J. M. Tour and N. A. Koratkar, *ACS Nano*, 2010, **4**, 7415–7420.
6 M. H. Wu, Y. Gao, Z. Y. Zhang and X. C. Zeng, *Nanoscale*, 2012, **4**, 915–920.
7 J. G. Son, M. Son, K. J. Moon, B. H. Lee, J. M. Myoung, M. S. Strano, M. H. Ham and C. A. Ross, *Adv. Mater.*, 2013, **25**, 4723–4728.
8 M. K. Liu, Y. F. Song, S. X. He, W. W. Tjiu, J. S. Pan, Y. Y. Xia and T. X. Liu, *ACS Appl. Mater. Interfaces*, 2014, **6**, 4214–4222.
9 S. S. Datta, D. R. Strachan, S. M. Khamis and A. T. C. Johnson, *Nano Lett.*, 2008, **8**, 1912–1915.
10 X. Y. Yang, X. Dou, A. Rouhanipour, H. J. Räder and K. Müllen, *J. Am. Chem. Soc.*, 2008, **130**, 4216–4217.
11 Z. S. Wu, W. Ren, L. Gao, B. Liu, J. Zhao and H. M. Cheng, *Nano Res.*, 2010, **3**, 16–22.
12 L. Tapaszto, G. Dobrik, P. Lambin and L. P. Biro, *Nat. Nanotechnol.*, 2008, **3**, 397–401.
13 A. L. Higginbotham, D. V. Kosynkin, A. Sinitskii, Z. Z. Sun and J. M. Tour, *ACS Nano*, 2010, **4**, 2059–2069.
14 Z. Wu, D. Wang, W. Ren, J. Zhao, G. Zhou, F. Li and H. Cheng, *Adv. Funct. Mater.*, 2010, **20**, 3595–3602.
15 A. V. Talyzin, I. V. Anoshkin, A. V. Krasheninnikov, R. M. Nieminen, A. G. Nasibulin, H. Jiang and E. I. Kauppinen, *Nano Lett.*, 2011, **11**, 4352–4356.
16 Y. Li, W. Zhou, H. Wang, L. Xie, Y. Liang, F. Wei, J.-C. Idrobo, S. J. Pennycook and H. Dai, *Nat. Nanotechnol.*, 2012, **7**, 394–400.
17 C. L. Sun, C. T. Chang, H. H. Lee, J. G. Zhou, J. Wang, T. K. Sham and W. F. Pong, *ACS Nano*, 2011, **5**, 7788–7795.
18 G. B. Zhu, Y. H. Yi, Z. X. Han, K. Wang and X. Y. Wu, *Anal. Chim. Acta*, 2014, **845**, 30–37.
19 Y. G. Wu, F. Z. Wang, S. S. Zhan, L. Liu, Y. F. Luo and P. Zhou, *RSC Adv.*, 2013, **3**, 25614–25619.
20 L. Su, J. Feng, X. M. Zhou, C. L. Ren, H. H. Li and X. G. Chen, *Anal. Chem.*, 2012, **84**, 5753–5758.
21 Y. J. Song, W. L. Wei and X. G. Qu, *Adv. Mater.*, 2011, **23**, 4215–4236.
22 Y. L. Dong, H. G. Zhang, Z. U. Rahman, L. Su, X. J. Chen, J. Hu and X. G. Chen, *Nanoscale*, 2012, **4**, 3969–3976.
23 X. Xia, Y. Long and J. Wang, *Anal. Chim. Acta*, 2013, **772**, 81–86.
24 J. Xie, X. Zhang, H. Wang, H. Zheng and Y. Huang, *Trends Anal. Chem.*, 2012, **39**, 115–129.
25 L. Z. Gao, J. Zhuang, L. Nie, J. B. Zhang, Y. Zhang, N. Gu, T. H. Wang, J. Feng, D. L. Yang, S. Perrett and X. Y. Yan, *Nat. Nanotechnol.*, 2007, **2**, 577–583.
26 C. Ray, S. Dutta, S. Sarkar, R. Sahoo, A. Roy and T. Pal, *J. Mater. Chem. B*, 2014, **2**, 6097–6105.
27 R. Andre, F. Natalio, M. Humanes, J. Leppin, K. Heinze, R. Wever, H. C. Schroeder, W. E. G. Mueller and W. Tremel, *Adv. Funct. Mater.*, 2011, **21**, 501–509.
28 L. J. Chen, B. Sun, X. D. Wang, F. M. Qiao and S. Y. Ai, *J. Mater. Chem. B*, 2013, **1**, 2268–2274.
29 L. Z. Zhou, L. Kuai, W. Z. Li and B. Y. Geng, *ACS Appl. Mater. Interfaces*, 2012, **4**, 6463–6467.
30 Y. J. Song, X. H. Wang, C. Zhao, K. G. Qu, J. S. Ren and X. G. Qu, *Chem.—Eur. J.*, 2010, **16**, 3617–3621.
31 R. J. Cui, Z. D. Han and J. J. Zhu, *Chem.—Eur. J.*, 2011, **17**, 9377–9384.
32 Y. J. Song, K. G. Qu, C. Zhao, J. S. Ren and X. G. Qu, *Adv. Mater.*, 2010, **22**, 2206–2210.
33 Z. B. Wang, X. C. Lv and J. Weng, *Carbon*, 2013, **62**, 51–60.
34 W. B. Shi, Q. L. Wang, Y. J. Long, Z. L. Cheng, S. H. Chen, H. Z. Zheng and Y. M. Huang, *Chem. Commun.*, 2011, **47**, 6695–6697.
35 A. X. Zheng, Z. X. Cong, J. R. Wang, J. Li, H. H. Yang and G. N. Chen, *Biosens. Bioelectron.*, 2013, **49**, 519–524.
36 H. J. Sun, N. Gao, K. Dong, J. S. Ren and X. G. Qu, *ACS Nano*, 2014, **8**, 6202–6210.
37 S. R. Cao, L. Zhang, Y. Q. Chai and R. Yuan, *Biosens. Bioelectron.*, 2013, **42**, 532–538.
38 V. Raja, R. Jaimeb, D. Astrucb and K. Sreenivasana, *Biosens. Bioelectron.*, 2011, **27**, 197–200.
39 C. Zhao, L. Wan, L. Jiang, Q. Wang and K. Jiao, *Anal. Biochem.*, 2008, **383**, 25–30.
40 C. P. Wu, D. R. Ifa, N. E. Manicke and R. G. Cooks, *Anal. Chem.*, 2009, **81**, 7618–7624.
41 Y. J. Lee and J. Y. Park, *Biosens. Bioelectron.*, 2010, **26**, 1353–1358.
42 R. M. Li, C. Xiong, Z. Y. Xiao and L. S. Ling, *Anal. Chim. Acta*, 2012, **724**, 80–85.
43 M. Saghafi, F. Mahboubi, S. Mohajerzadeh, M. Fathi and R. Holze, *Curr. Appl. Phys.*, 2014, **14**, 1335–1343.
44 D. V. Kosynkin, A. L. Higginbotham, A. Sinitskii, J. R. Lomeda, A. Dimiev, B. K. Price and J. M. Tour, *Nature*, 2009, **458**, 872–876.
45 S. Stankovich, D. A. Dikin, R. D. Piner, K. A. Kohlhaas, A. Kleinhammes, Y. Jia, Y. Wu, S. T. Nguyen and R. S. Ruoff, *Carbon*, 2007, **45**, 1558–1565.
46 D. B. Shinde, J. Debgupta, A. Kushwaha, M. Aslam and V. K. Pillai, *J. Am. Chem. Soc.*, 2011, **133**, 4168–4171.
47 C. Nethravathi and M. Rajamathi, *Carbon*, 2008, **46**, 1994–1998.
48 B. J. Li, H. Q. Cao, J. Shao, M. Z. Qu and J. H. Warner, *J. Mater. Chem.*, 2011, **21**, 5069–5075.
49 S. H. Liu, F. Lu, R. M. Xing and J. J. Zhu, *Chem.–Eur. J.*, 2011, **17**, 620–625.
50 W. Q. Lai, J. Y. Zhuang, X. H. Que, L. B. Fu and D. P. Tang, *Biomater. Sci.*, 2014, **2**, 1073–1079.

51 Y. W. Hu, F. H. Li, X. X. Bai, D. Li, S. C. Hua, K. K. Wang and L. Niu, *Chem. Commun.*, 2011, **47**, 1743–1745.
52 X. H. Wang, K. G. Qu, B. L. Xu, J. S. Ren and X. G. Qu, *Nano Res.*, 2011, **4**, 908–920.
53 J. X. Xie, H. Y. Cao, H. Jiang, Y. J. Chen, W. B. Shi, H. Z. Zheng and Y. M. Huang, *Anal. Chim. Acta*, 2013, **796**, 92–100.
54 C. Xu, C. Q. Zhao, M. Li, L. Wu, J. S. Ren and X. G. Qu, *Small*, 2014, **10**, 1841–1847.
55 L. Su, J. Feng, X. M. Zhou, C. L. Ren, H. H. Li and X. G. Chen, *Anal. Chem.*, 2012, **84**, 5753–5758.
56 G. L. Luque, M. I. Rojasa, G. A. Rivas and E. P. M. Leiva, *Electrochim. Acta*, 2010, **56**, 523–530.
57 Y. Ma, M. G. Zhao, B. Cai, W. Wang, Z. Z. Ye and J. Y. Huang, *Chem. Commun.*, 2014, **50**, 11135–11138.
58 H. Zheng, H. G. Xue, Y. F. Zhang and Z. Q. Shen, *Biosens. Bioelectron.*, 2002, **17**, 541–545.